Interface Reaction between An Electroless Ni-Sn-P Metallization and Lead-free Sn-3.5Ag Solder with Suppressed Ni_3P Formation

Ying Yang,[1] J. N. Balaraju,[2] Yizhong Huang,[1] Yee Yan Tay,[1] Yiqiang Shen,[1] Zviad Tsakadze,[1] Zhong Chen[1]*

1-School of Materials Science and Engineering, Nanyang Technological University, Singapore 639798

2-Surface Engineering Division, CSIR National Aerospace Laboratories, Bangalore 560017, India

*Tel: +65-6790-4256; Email: aszchen@ntu.edu.sg

ABSTRACT

The voids formed in the Ni_3P layer during reaction between Sn-based solders and electroless Ni-P metallization is an important cause for the fast degradation of the solder joint reliability. To suppress the formation of Ni_3P phase, an electrolessly plated Ni-Sn-P alloy (6~7 wt.% of P and 19~21 wt.% of Sn) was developed to replace Ni-P in this study. The interfacial microstructure of electroless Ni-Sn-P/Sn-3.5Ag solder joints was investigated after reflow and solid-state aging. For comparison, the interfacial reaction in electroless Ni-P/Sn-3.5Ag solder joints under the same reflow and aging conditions was conducted. It was found that the Ni-Sn-P metallization is consumed much slower than the Ni-P metallization during soldering. After prolonged reaction, neither Ni_3P or voids are observed under SEM at the Ni-Sn-P/Sn-3.5Ag interface. Mainly, two intermetallic compounds (IMCs), Ni_3Sn_4 and $Ni_{13}Sn_8P_3$, are formed during the soldering reaction. The reason for the Ni_3P phase suppression and the overall reaction mechanisms at the Ni-Sn-P/Sn-3.5Ag interface are discussed.

*Keywords***:** Electroless Ni-Sn-P; Metallization; Interfacial reaction; Soldering; Intermetallic compound; Diffusion

INTRODUCTION

Electrolessly plated Ni-P has been widely used as soldering metallization materials for the past several decades. Accordingly, the interfacial reactions between electroless Ni-P and Sn-containing solders, as well as the implications to long-term reliability, have been widely studied and well understood [1-10]. During soldering, reaction between Sn and Ni activates the transformation of amorphous Ni-P metallization into a layer of crystalline Ni_3P containing numerous voids [11]. The formation mechanism of such voids has been explained too [1]. Since the Ni_3P layer has a fine columnar structure [1, 11-13], diffusion of Ni through this layer is much faster, leading to the accelerated interfacial reaction. As a result of the fast reaction, voids nucleate and grow in the Ni_3P layer after prolonged reaction [1, 4-7, 13], contributing to the weakened interface and degraded reliability of the solder joint. In order to slow down the interfacial reaction with lead-free solders, it is necessary to avoid the formation, or to suppress the growth of the fast diffusion path, the columnar Ni_3P layer. In previous studies, we developed electroless Ni-W-P [14] and Ni-Co-P [15] metallizations which show impressive slow-down of the interfacial reaction. During the Ni-W-P/Sn-3.5Ag interfacial reaction, a layer of amorphous $(Ni,W)_3P$ was formed with no voids in this layer, while in the case of Ni-Co-P/Sn-3.5Ag reaction, the addition of Co has changed the type, composition, and morphology of the intermetallic compounds (IMCs) formed at the interface. The success has prompted us to explore the use of other ternary elements to be added into electroless Ni-P and to investigate the mechanisms of the suppression of the fast reaction with lead-free solders. Since the voids-containing columnar Ni_3P layer is the weak link in the

diffusion barrier, a plausible strategy is to suppress the formation of the Ni_3P layer altogether through alloy design. According to the Ni-Sn-P phase diagram at 550 ℃ [16, 17], the formation of Ni_3P will be avoided when the Sn concentration is greater than ~10 wt. % (~5 at.%) when P content is around 6~7 wt.%. Instead, the composition falls into the region of (Ni + Ni_3Sn + $Ni_{21}P_6Sn_2$) at 550 °C [16]. In a private communication with C. Schmetterer, the author of references [16, 17], the Ni-Sn-P phase diagram for lower temperatures below 550 °C is not available due to a number of practical difficulties. In such event, no thermodynamic data can be obtained at the solder reflow temperature around 260 °C. Nevertheless we could hypothesize that if the ternary phase ($Ni_{21}P_6Sn_2$) is stable at lower temperatures, the three-phase equilibrium (Ni + Ni_3Sn + $Ni_{21}P_6Sn_2$) could be maintained without the presence of Ni_3P. This principle is true, even if the three phases are not exact as what they are at 550 °C.

To test the above hypothesis, Ni-P alloy with incorporation of a high content of Sn was prepared for soldering reaction with Sn-3.5Ag. Interfacial reaction between Ni-Sn-P and Sn-3.5Ag solder after reflow and prolonged aging was studied. The diffusional formation mechanism of IMCs at the Ni-Sn-P/Sn-3.5Ag interface was proposed as well. For comparison, the interfacial reaction between the same solder and a binary electroless Ni-P metallization under the same reflow and aging conditions was carried out.

EXPERIMENTAL PROCEDURES

Cu plates (6 mm thick, 99.98 wt.%) were used as substrate for electroless plating of both Ni-P and Ni-Sn-P. Prior to plating, the Cu surface was activated by using a commercial ruthenium-based pre-initiator. Electroless Ni-P plating was conducted in a commercial acidic sodium hypophosphite bath (from MacDermid) with a pH level of 5.3 at 88 ± 2 ºC for 40

mins. Electroless Ni-Sn-P plating was performed in an alkaline bath with a pH level of 9.0 at 88 ± 2 ºC for 30 mins. As listed in Table I, the Ni-Sn-P plating bath contains nickel sulphate and sodium stannate as nickel and tin sources respectively, sodium hypophosphite as reducing agent along with complexing agents and buffering agents.

The electrolessly coated Cu plates were joined by lead-free Sn-3.5Ag solder to form Ni-P/Sn-3.5Ag and Ni-Sn-P/Sn-3.5Ag solder joints. Prior to the joining, a thin layer of no-clean paste flux was applied on top of the plated surface of Cu to remove oxides. Commercially obtained Sn-3.5Ag solder wires with flux in core were used for the soldering. The reflow soldering process was conducted in an IR reflow oven (ESSEMTEC RO-06E) with a peak temperature of 260 °C for 60 s, followed by solid-state aging at 200 °C for up to 200 h.

The surface morphologies and the thicknesses of both Ni-P and Ni-Sn-P coating layers were observed under scanning electron microscope (SEM), along with the interfacial microstructures of both types of solder joints after prolonged aging at 200 °C. The compositions of the as-deposited, the as-reflowed and the aged samples were analyzed using energy dispersive X-ray (EDX) incorporated in the SEM. For the cross-sectional SEM study, samples were cold mounted in epoxy and polished down to 1 μm finish, followed by etching with 4% hydrochloric acid to reveal the interfacial microstructure. Moreover, the newly-formed interfacial compound in the Ni-Sn-P/Sn-3.5Ag solder joint was identified by using transmission electron microscope (TEM). The TEM sample was prepared by focused ion beam (FIB) technique.

RESULTS

As-deposited Metallizations

The composition of the deposited Ni-P layer was measured to be 6~7 wt.% of P by EDX. As shown in Fig. 1(a), the surface of the Ni-P layer had smooth nodules with uneven size. The thickness of the Ni-P layer was around 14 μm (Fig. 1(b)). The deposited Ni-Sn-P layer contained 6~7 wt.% P and 19~21 wt.% Sn. It was observed that the Ni-Sn-P layer had a very similar surface morphology as the Ni-P deposit (Fig. 2(a)). The Ni-Sn-P layer had a thickness around 12.1 μm (Fig. 2(b)). It was noted that both coatings have a good adhesion to the Cu substrate (Figs. 1(b) & 2(b)).

Liquid-state Interfacial Reactions during Reflow

Fig. 3(a) shows the cross-sectional micrograph of the as-reflowed Ni-P/Sn-3.5Ag solder joint. Chunky-shaped Ni_3Sn_4 is the primary IMC formed at the joint interface, and some of them spalled into the bulk solder. The formation of Ni_3Sn_4 is due to the reaction between Sn from the solder and Ni from the Ni-P metallization. A dark layer of Ni_3P formed within the top region of the Ni-P metallization, with a few voids present inside. The formation of these voids has been explained in previous study [1]. A very thin ternary Ni_2SnP layer was also noticed to be present in between the Ni_3Sn_4 and Ni_3P layers [6, 18].

For the as-reflowed Ni-Sn-P/Sn-3.5Ag solder joint, chunky-shaped Ni_3Sn_4 was formed (Fig. 3(b)). Unlike at the as-reflowed Ni-P/Sn-3.5Ag interface, there was neither Ni_3P layer nor voids formed at the as-reflowed Ni-Sn-P/Sn-3.5Ag interface. Thus, the hypothesis is confirmed that the formation of Ni_3P layer could be avoided through the design of the metallization composition. From Fig. 3(b), a thin layer of ternary Ni-Sn-P compound was

also observed in between the Ni_3Sn_4 layer and the unconsumed Ni-Sn-P metallization. EDX result indicates that this newly-formed ternary Ni-Sn-P compound contains ~51 at.% Ni, ~34 at.% Sn and ~15 at.% P. It is a different type of IMC from the Ni_2SnP compound formed at the Ni-P/Sn-3.5Ag interface. The phase identification will be discussed later.

It is noticed that the plated Ni-Sn-P layer shows a clear "tree-like" morphology (Fig. 3(b)). Within this amorphous layer (to be discussed later), the morphological contrast is due to composition variation, which has been observed in electroless Ni-P plating [19]. The reason for the compositional variation was explained in the literature by the periodical fluctuation in the pH of the plating solution adjacent to the deposited surface. It is known that the composition of electrolessly plated Ni-P alloy is very sensitive to the solution pH value. The fluctuation in pH is caused by hydrogen evolution and the reduction of hypophosphite, which decreases the "local" pH value. It takes some time for the solution at the "local" metal / solution interface to recover the composition of the bulk solution through diffusion. Therefore such localized depletion / replenish cycle typically leads to a lamellar type of morphology in Ni-P plating [19]. In the current work, the Ni-Sn-P layer follows a columnar growth pattern. Such growth pattern, coupled with the pH fluctuation during plating, has caused the unique "tree-like" morphology in the Ni-Sn-P layer. EDX line scan (not shown here) indicates that the dark region has a higher P and lower Sn concentration, while Ni concentration remains constant throughout the coating thickness. The compositional variation may be harmful to the long-term solder joint reliability; future work is needed to homogenize the layer composition through bath formulation and adjustment of plating conditions.

Solid-state Interfacial Reactions during Aging

Fig. 4(a) and 4(b) show the growth of various compounds at the Ni-P/Sn-3.5Ag interface after aging at 200 °C for 50 h and 200 h, respectively. The Ni_3Sn_4 layer grew much thicker upon aging, with some Ag_3Sn particles accumulated inside. After aging for 50 h, the Ni-P metallization was fully consumed and transformed into Ni_3P layer (Fig. 4(a)). The thickness of the Ni_3P layer (~7.4 μm) is much smaller than that of the as-deposited Ni-P layer (~14 μm). Such shrinkage indicates that Ni atoms diffuse out from Ni-P to form Ni_3Sn_4 during soldering reaction. After 200 h of aging, the thickness of the Ni_3P layer (~5.8 μm) was reduced by around 20% as compared to that after 50 h of aging (~7.4 μm), while the thickness of the Ni_2SnP layer increased to around 3 times the one after 50 h of aging. This indicates that, once the Ni-P layer is fully consumed, the Ni_2SnP layer grows rapidly at the expense of the Ni_3P layer [6]. There were only a few voids present in the Ni_3P layer at the as-reflowed state (Fig. 3(a)); however, as the reaction proceeded upon aging, the voids in the Ni_3P layer grew both in size and number (Fig. 4(a) and 4(b)). Interestingly, after the Ni-P metallization was fully consumed (Fig. 4(a) and 4(b)), instead of $(Ni,Cu)_3Sn_4$, only Ni_3Sn_4 formed and no voids were observed at the Cu/Ni_3P interface, indicating that Cu atoms still remained in the substrate even after aging for 200 h.

Fig. 4(c) and 4(d) show the growth of various compounds at the Ni-Sn-P/Sn-3.5Ag interface after aging at 200 °C for 50 h and 200 h, respectively. Some Ag_3Sn particles were observed to accumulate inside the Ni_3Sn_4 layer. During prolonged aging, the growth of the Ni_3Sn_4 layer at the Ni-Sn-P/Sn-3.5Ag interface was much slower than that at the Ni-P/Sn-3.5Ag interface. After 50 h of aging, around 3.3 μm of the Ni-Sn-P metallization was consumed. As a comparison, the Ni-P metallization with an original thickness of around 14 μm was fully consumed after aging for 50 h (Fig. 4(a)). Even after 200 h of aging (Fig. 4(d)),

only around 5.4 μm Ni-Sn-P metallization was consumed, indicating that the Ni-Sn-P metallization was consumed much slower than the Ni-P metallization. The significantly reduced consumption rate of the Ni-Sn-P metallization is consistent with the much reduced growth rate of the Ni_3Sn_4 layer as compared to that at the Ni-P/Sn-3.5Ag interface. It is worth mentioning that no Ni_3P was observed at the Ni-Sn-P/Sn-3.5Ag interface with extended aging for up to 200 h (Fig. 4(d)), indicating that this phase is thermodynamically avoidable. Moreover, the growth of the Ni-Sn-P compound at the Ni-Sn-P/Sn-3.5Ag interface was negligible during aging.

Identification of the Newly-formed Ni-Sn-P IMC

The crystal structure of the newly-formed Ni-Sn-P compound at the Ni-Sn-P/Sn-3.5Ag interface was identified using electron diffraction under TEM. The TEM sample was prepared by FIB technique from the Ni-Sn-P/Sn-3.5Ag interface after reflow for 25 cycles (reflow at 260 °C for 60 s as one cycle). Fig. 5 shows the TEM micrograph of the FIB sample and the lattice image of the Ni-Sn-P compound. The EDX result of this compound from TEM is consistent with the result obtained from SEM. The lattice image of the Ni-Sn-P compound with the Fourier reconstructed pattern (Fig. 5(b)) is matched to $Ni_{13}Sn_8P_3$, combined with the composition result from EDX as a secondary evidence, this new compound was identified as $Ni_{13}Sn_8P_3$ having a triclinic lattice (*P1*, a = 6.456 Å, b = 21.291 Å, c = 13.247 Å, α = 81.052°, β = 56.260°, γ = 68.221°) [20].

DISCUSSION

Only two interfacial compounds, Ni_3Sn_4 and $Ni_{13}Sn_8P_3$ are formed during the Ni-Sn-P/Sn-3.5Ag interfacial reaction. Since the Ni-Sn-P metallization itself contains both Ni and Sn, in order to determine whether the formation of Ni_3Sn_4 is caused by the soldering reaction between Sn from the solder and Ni from the metallization or the reaction between the existing Ni and Sn within the metallization at the reflow temperature, XRD was conducted on the as-deposited Ni-Sn-P after annealing at 260 ℃ (the same as the reflow temperature). Fig. 6 shows XRD patterns of the Ni-Sn-P deposit before and after annealing at 260 ℃ for 2 h. The XRD spectra were recorded between 2-theta from 30° to 80° with a fixed glancing angle of 2°. It was observed that the pattern for the as-deposited Ni-Sn-P consisted of only one broad peak with highest intensity belonging to Ni; hence, the as-deposited Ni-Sn-P had an amorphous structure. After annealing at 260 ℃ for 2 h, no peaks from Ni_3Sn_4 were present in the pattern, so the Ni-Sn-P deposit still had an amorphous structure, proving that the formation of Ni_3Sn_4 cannot occur by the reaction between the Sn and Ni composition within the Ni-Sn-P metallization itself. Therefore, the formation of Ni_3Sn_4 is caused by the reaction between the Sn atoms diffusing out from the solder and the Ni atoms diffusing out from the metallization during soldering between Ni-Sn-P and Sn-3.5Ag. Meanwhile, the continuous formation of Ni_3Sn_4 during soldering reaction leads to the depletion of Ni from the surface of the Ni-Sn-P metallization.

The $Ni_{13}Sn_8P_3$ compound has not been reported in any soldering systems, and this compound thickens as reaction proceeds. Here we propose a diffusional formation mechanism based on several observations in this work. From the literatures, it has been proven that there is no out-diffusion of P atoms from the Ni-P metallization during soldering reaction [1]. In this work, the P atoms in the Ni-Sn-P metallization are also believed to

remain in the metallization layer during soldering reaction. This is probably best confirmed by comparing the compositions of the as-deposited Ni-Sn-P layer (77 at.% Ni, 10 at.% Sn and 13 at.% P) and the newly-formed $Ni_{13}Sn_8P_3$ layer (54 at.% Ni, 33 at.% Sn and 13 at.% P based on the chemical formula). Since both layers have the similar P concentration, it is most likely that the Ni-Sn-P deposit is transformed into the $Ni_{13}Sn_8P_3$ compound during soldering reaction. As the Ni and Sn concentrations in the two neighboring layers are different, we need to explain the diffusion paths for these two elements during the solder reaction.

The formation of Ni_3Sn_4 causes depletion of Ni from the surface of the Ni-Sn-P layer, so the top region of the Ni-Sn-P layer is transformed into a phase with lower Ni concentration, which is in agreement with the fact that the $Ni_{13}Sn_8P_3$ compound has a lower Ni content than the Ni-Sn-P metallization. Since the $Ni_{13}Sn_8P_3$ compound has a higher Sn content than the Ni-Sn-P deposit, it is speculated that the transformation of the Ni-Sn-P deposit into the $Ni_{13}Sn_8P_3$ compound requires Sn supply from the solder, which is similar to the formation of the Ni_2SnP compound during the Ni-P/Sn-3.5Ag interfacial reaction [6, 21-24]. Based on the above arguments, we believe that the polycrystalline $Ni_{13}Sn_8P_3$ compound is formed by transforming the amorphous Ni-Sn-P metallization with the aid of outward diffusion of Ni and inward diffusion of Sn during the soldering reaction.

To support the proposed diffusional interface reaction mechanism, compositional area mapping was carried out on the Ni-Sn-P/Sn-3.5Ag interface after aging at 200 ºC for 200 h (Fig. 7), it was clearly seen that P atoms remained in the Ni-Sn-P and $Ni_{13}Sn_8P_3$ layers. In contrast, Ni atoms diffused out from the Ni-Sn-P layer to form Ni_3Sn_4. The signal from Sn atoms was detected in all layers, except the Cu substrate. These are in agreement with the aforementioned diffusional formation mechanism of Ni_3Sn_4 and $Ni_{13}Sn_8P_3$ compounds at the Ni-Sn-P/Sn-3.5Ag interface.

Fig. 8 schematically illustrates the diffusional formation mechanism of IMCs at the Ni-Sn-P/Sn-3.5Ag interface. The Sn atoms diffusing out from the solder react with the Ni atoms from the Ni-Sn-P metallization to form the Ni_3Sn_4 compound. Meanwhile, the top region of the Ni-Sn-P metallization becomes Ni-depleted due to the out-diffusion of Ni to form Ni_3Sn_4. Since Sn is the faster diffusant in Ni_3Sn_4 [25], some Sn atoms will also reach the Ni_3Sn_4/Ni-Sn-P interface to form the $Ni_{13}Sn_8P_3$ compound. The continued growth of Ni_3Sn_4 requires Ni supply from the Ni-Sn-P layer, so Ni atoms have to diffuse through the formed $Ni_{13}Sn_8P_3$ layer to react with the Sn atoms from the solder. As a further verification, we have applied the law of mass conservation at the Ni-Sn-P/Sn-3.5Ag interface to examine the thickness evolution among the Ni-Sn-P metallzation, Ni_3Sn_4, and $Ni_{13}Sn_8P_3$ layers. It is proven that all of the Ni atoms diffuse out from the Ni-Sn-P layer take part in the reaction to form Ni_3Sn_4, and the depletion of Ni from the surface of the Ni-Sn-P layer leads to the formation of the $Ni_{13}Sn_8P_3$ layer (details are omitted in this paper).

The avoidance of the porous columnar Ni_3P layer is the reason for the slower interface reaction in the case of Ni-Sn-P metallization. In the case of Ni-P metallization, the Ni_2SnP IMC layer in between the Ni_3Sn_4 IMC and the Ni-P metallization is void-free and thus could be an effective diffusion barrier too. However the Ni_2SnP layer thickness remains very thin until the Ni-P metallization is fully consumed; after which it rapidly grows by “consuming” the existing Ni_3P layer with inherited voids [6]. Thus, the Ni2SnP layer has limited ability as a diffusion barrier. In the case of Ni-Sn-P, although the $Ni_{13}Sn_8P_3$ layer is also thin within the aging treatment duration, the elimination of the fast diffusion Ni_3P layer leads to such a large difference in the metallization consumption rate between the Ni-P and Ni-Sn-P. In other words, the good diffusion barrier performance displayed by the Ni-Sn-P metallization is

achieved not by adding a better-performing barrier layer, but by eliminating the worst-performing Ni_3P layer.

CONCLUSIONS

In this study, an electrolessly plated Ni-Sn-P alloy (6~7 wt.% of P and 19~21 wt.% of Sn) has been developed as an alternative Ni-based metallization for lead-free soldering. Interfacial reaction between Sn-3.5Ag solder and electroless Ni-Sn-P after reflow and aging was investigated, with interfacial reaction between the same solder and electroless Ni-P (6~7 wt.% of P) under the same reflow and aging conditions as a benchmark. Only two intermetallic compounds, Ni_3Sn_4 and $Ni_{13}Sn_8P_3$ are formed during the Ni-Sn-P/Sn-3.5Ag interfacial reaction. The Sn atoms from the solder react with the Ni atoms from the Ni-Sn-P metallization to form Ni_3Sn_4, and as a result, the top surface of the metallization layer becomes Ni-depleted. The Sn atoms from the solder also diffuse through the formed Ni_3Sn_4 layer to reach the Ni_3Sn_4/Ni-Sn-P interface, and react with the Ni-depleted region of the Ni-Sn-P layer to form the second IMC-$Ni_{13}Sn_8P_3$. Such reaction mechanism has been proven by the mass balance of Ni during Ni-Sn-P/Sn-3.5Ag interfacial reaction, which confirms that all of the Ni atoms diffused out from the Ni-Sn-P layer take part in the reaction to form Ni_3Sn_4. With successful elimination of the fast diffusion path, which is the columnar Ni_3P layer, the Ni-Sn-P metallization was consumed much slower than the Ni-P metallization. Therefore, electroless Ni-Sn-P alloy with a high Sn content is a promising metallization material for lead-free soldering.

ACKNOWLEDGEMENT

Financial assistance from Ministry of Education (MOE) of Singapore (grant RG 19/00, RG 14/03) is gratefully acknowledged.

REFERENCES

[1] M. He, Z. Chen, G.J. Qi, Acta Mater. 52, 2047 (2004).

[2] M. He, A. Kumar, P.T. Yeo, G.J. Qi, Z. Chen, Thin Solid Films 462-463, 387 (2004).

[3] M. He, Z. Chen, G.J. Qi, C.C. Wong, S.G. Mhaisalkar, Thin Solid Films 462-463, 363 (2004).

[4] A. Kumar, M. He, Z. Chen, Surf. Coat. Technol. 198, 283 (2005).

[5] A. Kumar, Z. Chen, S.G. Mhaisalkar, C.C. Wong, P.S. Teo, V. Kripesh, Thin Solid Films 504, 410 (2006).

[6] A. Kumar, Z. Chen, J. Electron. Mater. 40, 213 (2011).

[7] H.B. Kang, J.H. Bae, J.W. Yoon, S.B. Jung, J. Park, C.W. Yang, Scr. Mater. 64, 597 (2011).

[8] M. He, W.H. Lau, G.J. Qi, Z. Chen, Thin Solid Films 462-463, 376 (2004).

[9] M. He, Z. Chen, G.J. Qi, Metall. Mater. Trans. A 36, 65 (2005).

[10] Mona, A. Kumar, Z. Chen, IEEE Trans. Adv. Pack. 30, 68 (2007).

[11] J.W. Jang, P.G. Kim, K.N. Tu, D.R. Frear, P. Thompson, J. Appl. Phys. 85, 8456 (1999).

[12] P.L. Liu, Z.K. Xu, J.K. Shang, Metall. Mater. Trans. A 31, 2857 (2000).

[13] K. Zeng, K.N. Tu, Mater. Sci. Eng., R 38, 55 (2002).

[14] Y. Yang, J.N. Balaraju, S.C. Chong, H. Xu, C. Liu, V.V. Silberschmidt, Z. Chen, J. Alloys Compd. 565, 11 (2013).

[15] Y. Yang, J.N. Balaraju, Y. Z. Huang, H. Liu, Z. Chen, Acta Mater. 71, 69 (2014).

[16] C. Schmetterer, J. Vizdal, A. Kroupa, A. Kodentsov, H. Ipser, J. Electron. Mater. 38, 2275 (2009).

[17] C. Schmetterer, H. Ipser, Metall. Mater. Trans. A 41, 43 (2010).

[18] Z. Chen, M. He, G.J. Qi, J. Electron. Mater. 33, 1465 (2004).

[19] Z. Chen, X. Xu, C. C. Wong, S. Mhaisalkar, Surf. Coat. Tech. 167, 170 (2003)

[20] F.J. García-García, A.K. Larsson, S. Furuseth, Solid State Sci. 5, 205 (2003).

[21] Y.C. Lin, T.Y. Shih, S.K. Tien, J.G. Duh, Scr. Mater. 56, 49 (2007).

[22] Y.C. Lin, J.G. Duh, Scr. Mater. 54, 1661 (2006).

[23] Y.C. Lin, T.Y. Shih, S.K. Tien, J.G. Duh, J. Electron. Mater. 36, 1469 (2007).

[24] Y.C. Lin, K.J. Wang, J.G. Duh, J. Electron. Mater. 39, 283 (2010).

[25] C.E. Ho, S.C. Yang, C.R. Kao, J. Mater. Sci.: Mater. Electron. 18, 155 (2007).

Figure captions

Fig. 1. As-deposited Ni-P layer: (a) surface morphology, (b) cross-sectional micrograph

Fig. 2. As-deposited Ni-Sn-P layer: (a) surface morphology, (b) cross-sectional micrograph

Fig. 3. Back-scattered SEM images showing IMCs formed in the as-reflowed solder joints: (a) Ni-P/Sn-3.5Ag solder joint, and (b) Ni-Sn-P/Sn-3.5Ag solder joint

Fig. 4. Back-scattered SEM images showing IMCs formed in the aged solder joints: Ni-P/Sn-3.5Ag solder joint after aging at 200 °C for (a) 50 h and (b) 200 h; Ni-Sn-P/Sn-3.5Ag solder joint after aging at 200 °C for (c) 50 h and (d) 200 h

Fig. 5. (a) TEM micrograph showing the Ni-Sn-P/Sn-3.5Ag interface after reflow for 25 cycles, and (b) lattice image and Fourier reconstructed pattern of region A in (a) with $Ni_{13}Sn_8P_3$

Fig. 6. XRD patterns of the Ni-Sn-P coating before and after annealing at 260 ℃ for 2 h

Fig. 7. EDX element mapping analysis of the Ni-Sn-P/Sn-3.5Ag interface after aging at 200 ºC for 200 h: (a) SEM image, (b) mapping for Ni, (c) mapping for Sn, (d) mapping for P, (e) mapping for Cu, and (f) mapping for Ag. Elemental concentration decreases with decreasing colour intensity

Fig. 8. A schematic illustration of the diffusional mechanism of IMC formation at the Ni-Sn-P/Sn-3.5Ag interface

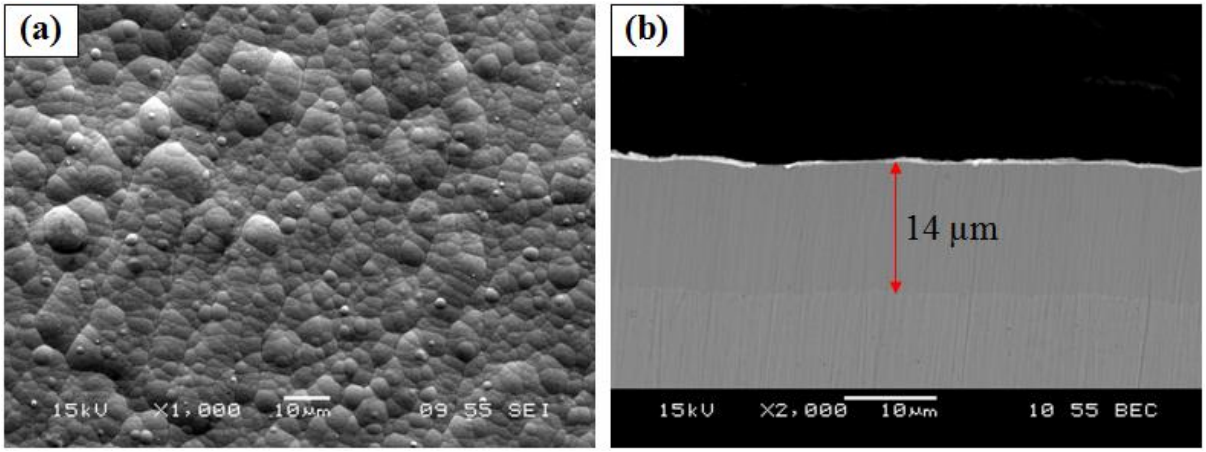

Fig. 1. As-deposited Ni-P layer: (a) surface morphology, (b) cross-sectional micrograph

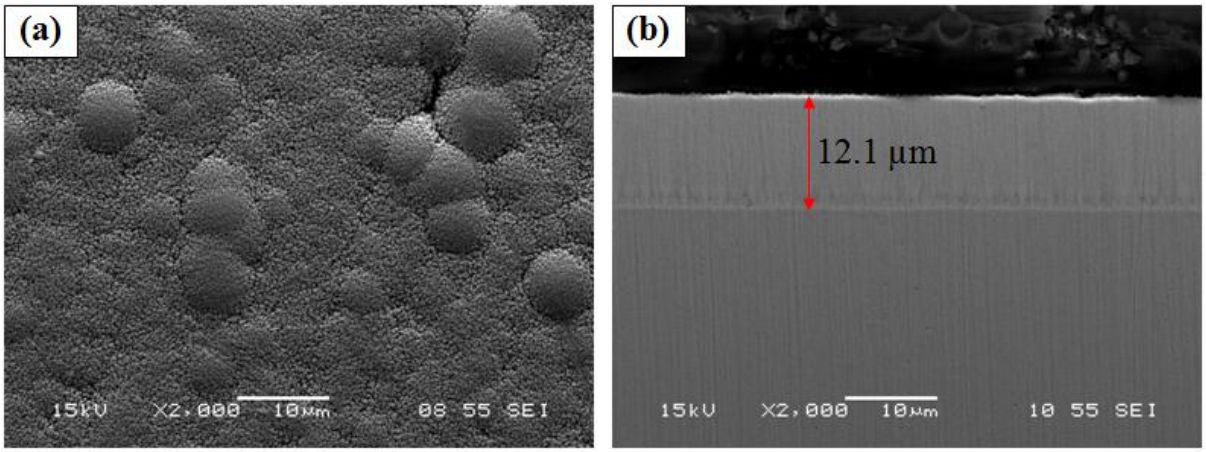

Fig. 2. As-deposited Ni-Sn-P layer: (a) surface morphology, (b) cross-sectional micrograph

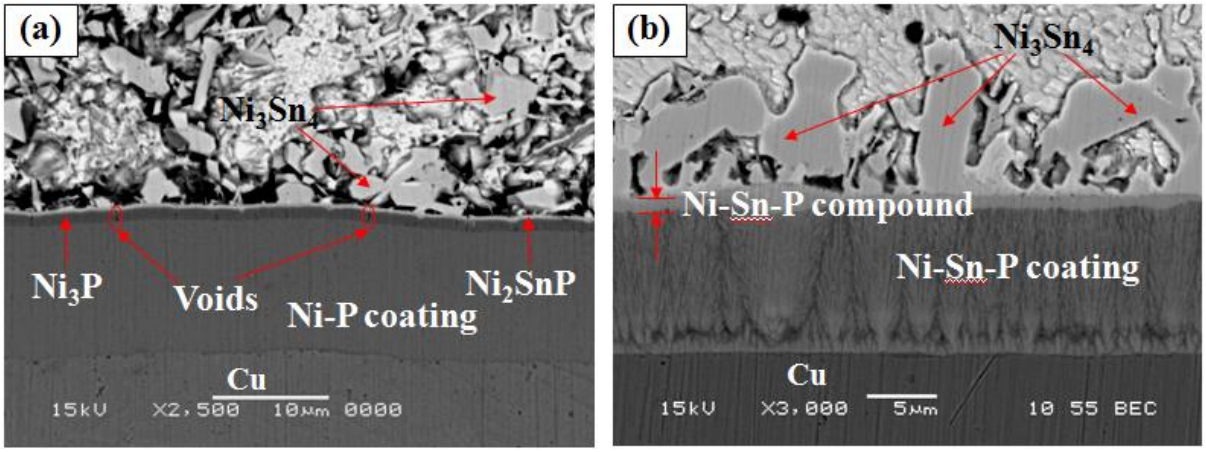

Fig. 3. Back-scattered SEM images showing IMCs formed in the as-reflowed solder joints: (a) Ni-P/Sn-3.5Ag solder joint, and (b) Ni-Sn-P/Sn-3.5Ag solder joint

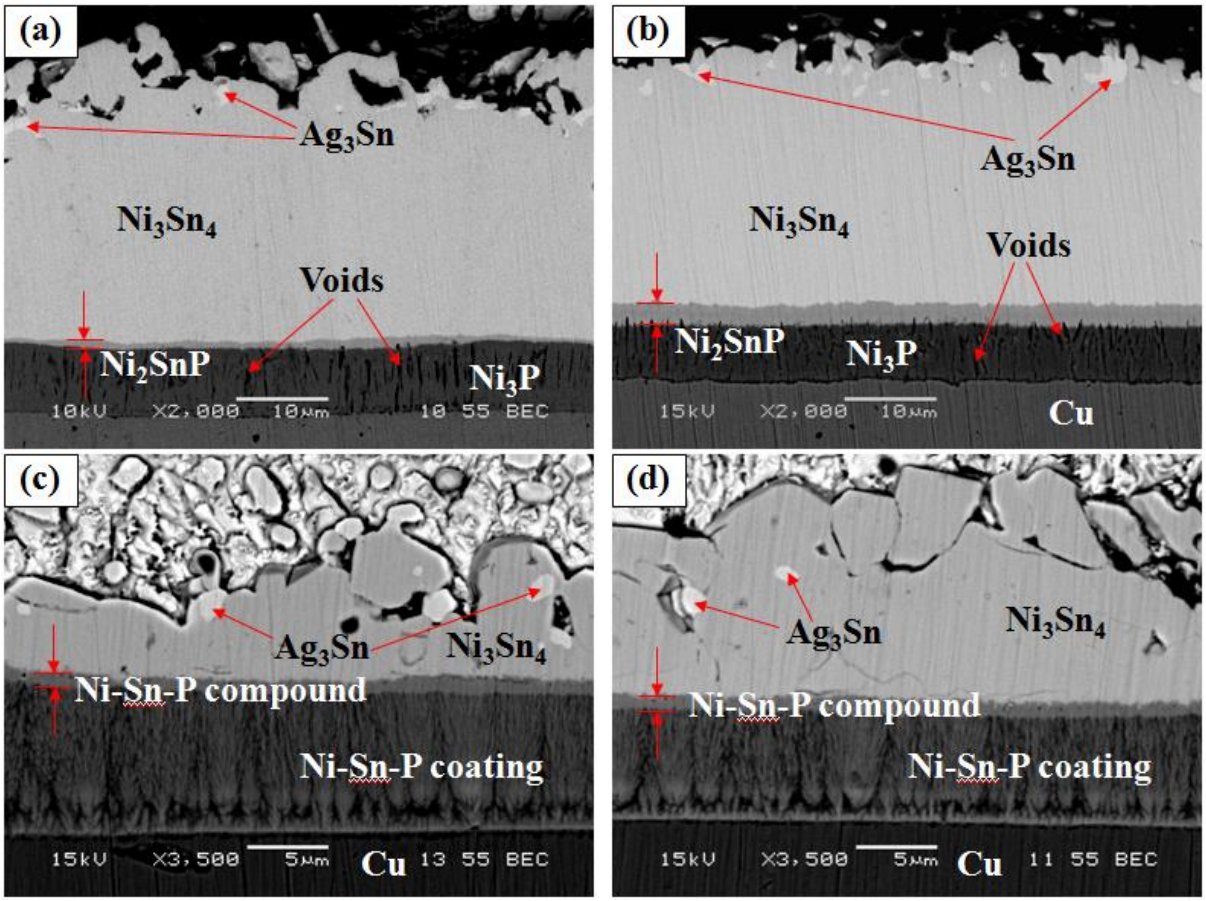

Fig. 4. Back-scattered SEM images showing IMCs formed in the aged solder joints: Ni-P/Sn-3.5Ag solder joint after aging at 200 °C for (a) 50 h and (b) 200 h; Ni-Sn-P/Sn-3.5Ag solder joint after aging at 200 °C for (c) 50 h and (d) 200 h

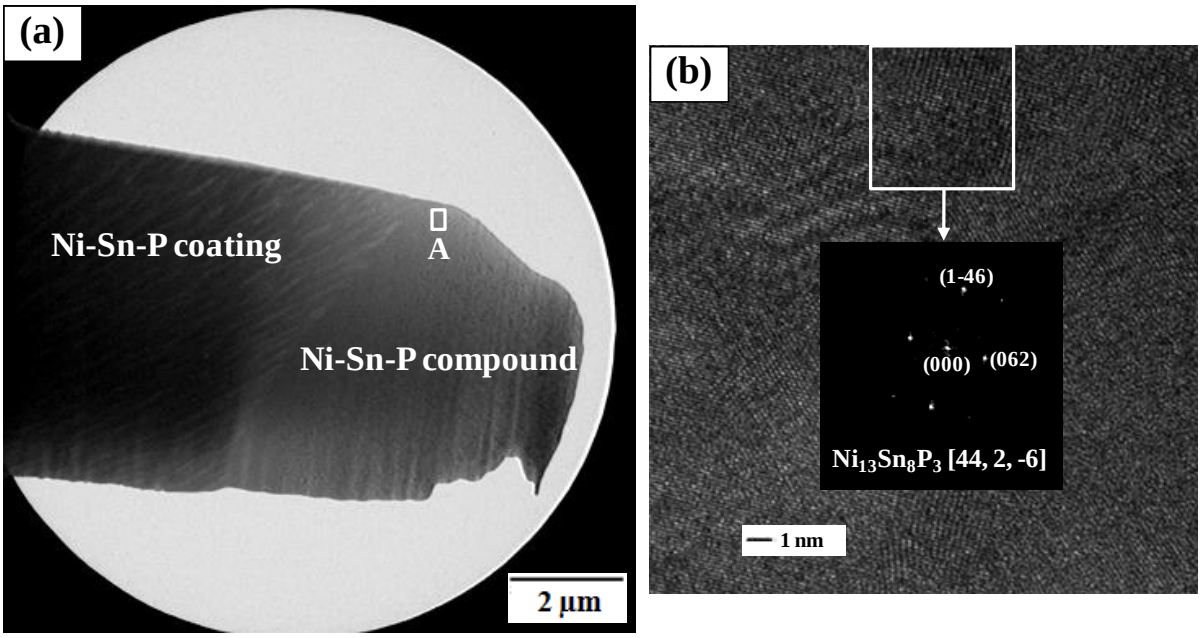

Fig. 5. (a) TEM micrograph showing the Ni-Sn-P/Sn-3.5Ag interface after reflow for 25 cycles, and (b) lattice image and Fourier reconstructed pattern of region A in (a) with $Ni_{13}Sn_8P_3$

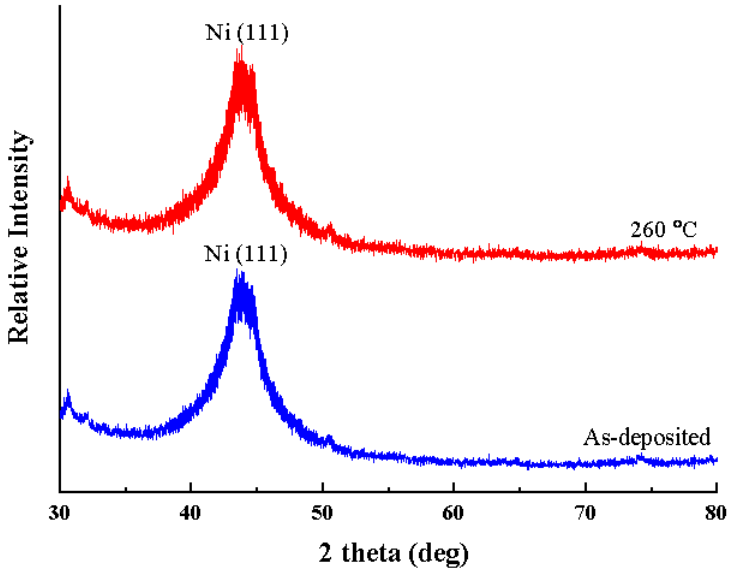

Fig. 6. XRD patterns of the Ni-Sn-P coating before and after annealing at 260 °C for 2 h

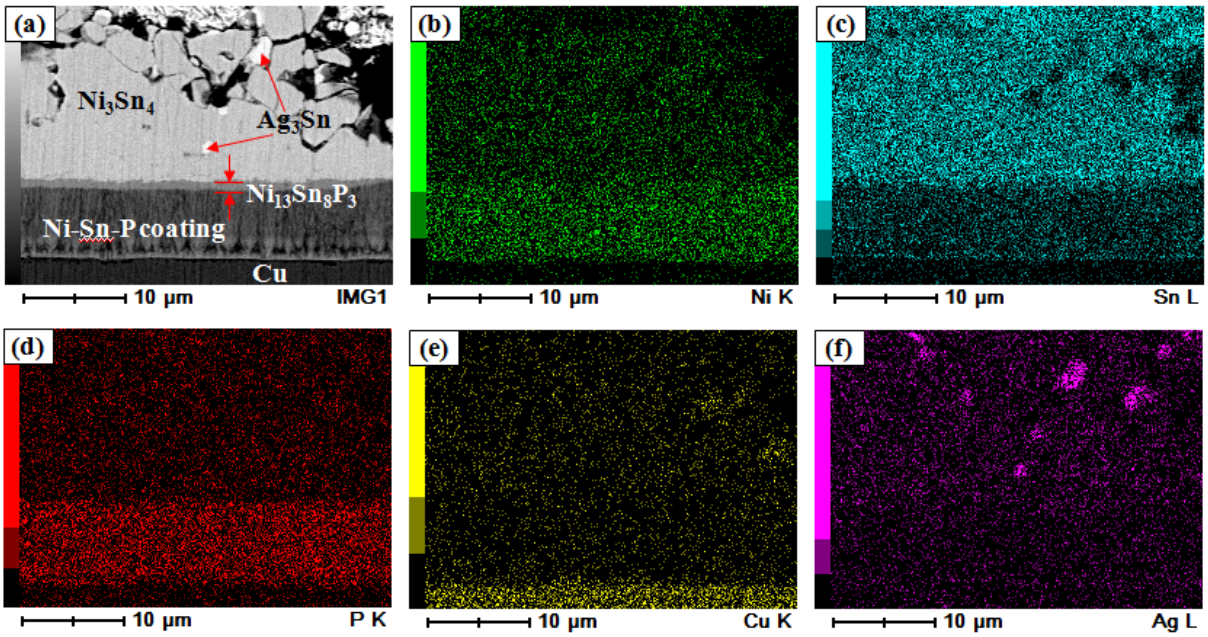

Fig. 7. EDX element mapping analysis of the Ni-Sn-P/Sn-3.5Ag interface after aging at 200 ºC for 200 h: (a) SEM image, (b) mapping for Ni, (c) mapping for Sn, (d) mapping for P, (e) mapping for Cu, and (f) mapping for Ag. Elemental concentration decreases with decreasing colour intensity

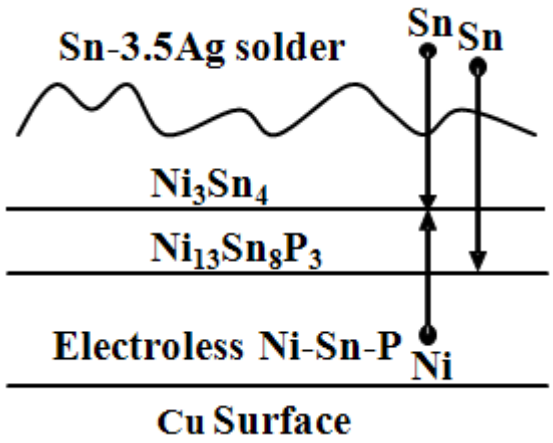

Fig. 8. A schematic illustration of the diffusional mechanism of IMC formation at the Ni-Sn-P/Sn-3.5Ag interface